12.5 HIGH RESOLUTION ANALYSES OF THE 8 MAY 2003 OKLAHOMA CITY STORM. PART II: EnKF DATA ASSIMILATION AND FORECAST EXPERIMENTS

David C. Dowell[1], Louis J. Wicker[2], and David J. Stensrud[2]
[1] Cooperative Institute for Mesoscale Meteorological Studies, Norman, OK
[2] National Severe Storms Laboratory, Norman, OK

1. INTRODUCTION

The ensemble Kalman filter (EnKF; Evensen 1994; Houtekamer and Mitchell 1998) is currently being tested as a method for retrieving the wind, thermodynamic, and microphysical fields in convective storms from radar observations (Snyder and Zhang 2003; Zhang et al. 2004; Dowell et al. 2004; Tong and Xue 2004). Applications for such retrievals include diagnosing storm processes and initializing numerical storm-scale forecast models. The EnKF technique for storm-scale retrieval is being refined according to the results of both Observing System Simulation Experiments (OSSEs) and real-data experiments.

We are currently applying the EnKF method to a real-data case – the 8 May 2003 supercell thunderstorm that produced an F4 tornado in Oklahoma City, Oklahoma. During the afternoon of 8 May 2003, several convective cells formed along a dryline in west-central Oklahoma (Fig. 1). Of these cells, only one evolved into a tornadic supercell (Burgess 2004). The life cycle of the Oklahoma City storm was documented by the KOUN radar, a 10-cm dual-polarization research Doppler radar in Norman, Oklahoma. By assimilating Doppler velocity and reflectivity observations from the KOUN radar into a numerical cloud model during the storm's development stage and then producing 40-min forecasts, we aim to (1) understand the storm evolution during the development state, and (2) determine how well the storm evolution during the tornadogenesis stage can be predicted.

2. ASSIMILATION EXPERIMENTS

Volume scans of Doppler velocity and effective reflectivity factor (hereafter "reflectivity") of the Oklahoma City storm were obtained by the KOUN radar approximately every 6 min. (Dual-polarization measurements were also collected but are not used in this study.) In our experiments, the 6 volumes between 2048 and 2126 UTC are assimilated into the model. These observations document the early stages of the Oklahoma City storm's life cycle, from "first echoes" to elongated cells with high-reflectivity cores (Fig. 1). The developing Oklahoma City storm was 50-80 km from the KOUN radar during this stage. A noteworthy feature of this dataset relative to another case studied by Dowell et al. (2004) is that widespread clear-air velocity data in the boundary layer are available (Fig. 1).

Before objectively analyzing the observations, we removed contaminated data (ground clutter, range folding, etc.) and unfolded aliased Doppler velocities. We used a Cressman scheme with a 1000-m radius of influence to analyze Doppler velocity and reflectivity at grid points 2000-m apart in the horizontal (Dowell et al. 2004); we analyzed each sweep (elevation angle) separately. Unlike Dowell et al. (2004), we assimilated each sweep at the time it was collected rather than assuming that the entire volume (consisting of 14 sweeps) was collected simultaneously. The interval between consecutive sweeps was 15-40 s.

The numerical cloud model used for the data-assimilation and forecast experiments is the NSSL Collaborative Model for Multiscale Atmospheric Simulation (NCOMMAS; Wicker and Wilhelmson

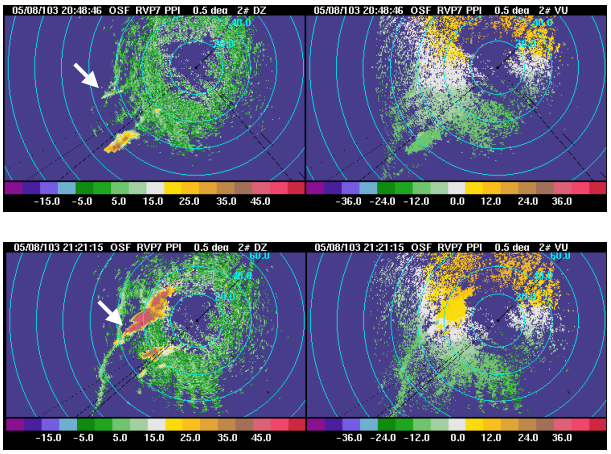

Figure 1. KOUN effective reflectivity factor (dBZ_e; left) and Doppler velocity (m s^{-1}; right) at 0.5° elevation angle at 20:48:46 UTC (top) and 21:21:15 UTC (bottom) 8 May 2003. The developing Oklahoma City storm is indicated by an arrow. The range rings are at 20-km intervals.

Corresponding author address: David C. Dowell, Cooperative Institute for Mesoscale Meteorological Studies, 1313 Halley Circle, Norman, OK, 73069; David.Dowell@noaa.gov

1995). Since 1995, the model has been updated to include the following features: third-order Runge-Kutta time integration, fifth-order (third-order) horizontal (vertical) differencing for advection, and a prognostic TKE scheme for turbulent mixing. The model also includes multiple options for precipitation microphysical schemes. The assimilation and forecast experiment described here is based on the modified (Gilmore et al. 2004) Lin-Farley-Orville (LFO) scheme (Lin et al. 1983), which includes four hydrometeor classes: rain, ice crystals, snow, and hail/graupel. At the conference, we will discuss the sensitivity of the results to the microphysical scheme parameters.

For the data-assimilation and forecast experiments, we employ a stationary grid consisting of 151 grid points (150 km) in each horizontal direction and 61 grid points (18 km) in the vertical direction. The horizontal grid spacing is uniformly 1 km, whereas the vertical grid spacing varies from 0.1 km in the lowest 1 km AGL to 0.7 km near the grid top. The grid origin is at the KOUN radar site, and the grid is positioned so that initial storm development (cf. Fig. 1) occurs in the southwest part of the domain (Fig. 2).

The environmental profile in the model (Figs. 3 and 4) is derived from the 0Z 9 May 2003 Norman, Oklahoma sounding, which was taken from very near the KOUN radar site (Fig. 2). The following modifications were made to the original sounding: a cap at 850 mb was weakened by decreasing the temperature by as much as 1.6 C between 850 and 720 mb, and the humidity around 770 mb was increased. These changes were motivated by earlier idealized experiments, which indicated that simulations (without data assimilation) initialized with a warm bubble at low levels had difficulty sustaining convection in the presence of the stronger cap. We are currently conducting data-assimilation experiments with the unmodified Norman sounding and will describe these experiments in a later paper. The following parameters in the modified sounding support supercellular convection: 3200 J kg^{-1} CAPE and 0.005 s^{-1} bulk vertical shear of the horizontal wind (30 m s^{-1} wind-vector difference) in the lowest 6 km AGL.

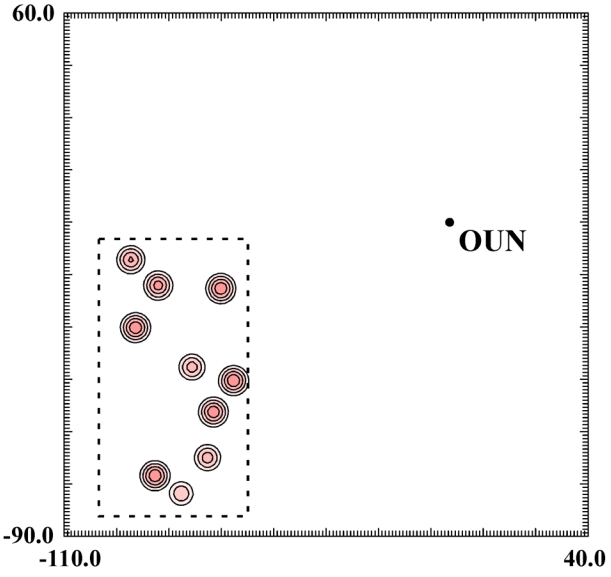

Figure 2. Perturbation temperature (contours and shading at intervals of 1.0 K) at 1.3 km AGL in the initial state of ensemble member 2. The perturbations have been added to a 40 km × 80 km portion of the 150 km × 150 km domain. The grid coordinates (km) are relative to the KOUN radar site ("OUN").

The initialization of each member of the 50-member forecast ensemble begins with the environmental profile in Fig. 3. Then, random sinusoidal perturbations are added to the vertical profile of each horizontal wind component (W. Skamarock and C. Snyder 2004, personal communication). The motivation for adding these horizontal-wind perturbations is uncertainty in the environmental conditions; in future experiments, one might also consider perturbing the environmental temperature and humidity profiles.

5-K warm bubbles at random locations within a limited portion of the domain ($-100 \le x \le -60$ km, $-85 \le y \le -5$ km, $0.25 \le z \le 2.25$ km) are then added to each ensemble member (Fig. 2); the region where the perturbations are added includes the region where radar echoes actually developed near the dryline (Fig. 1). Finally, each ensemble member is integrated 20 min before the first radar observation is assimilated; during this time, some of the warm bubbles initiate convective cells with precipitation aloft. The convective initiation mechanism in our experiment is artificial because the dryline is not actually modeled. Since important variability in the storm's environment such as that associated with the dryline is not represented in the model, one might expect limited predictability in this idealized experiment.

Both Doppler velocity (Dowell et al. 2004) and reflectivity observations (Tong and Xue 2004) are assimilated into the model. Observation errors are assumed to be 2 m s^{-1} and 5 dBZ for Doppler velocity and reflectivity, respectively. Although the latter error magnitude seems unrealistically large, we find that it is helpful to assume a large error magnitude when assimilating reflectivity observations. Observations are processed serially (that is, one at a time), and all model fields except pressure and the mixing coefficient are updated each time an observation is processed. Reflectivity corresponding to the model fields is computed in a manner similar to that described by Tong

and Xue (2004). No ensemble inflation is employed during the assimilation. Other details of the EnKF assimilation scheme are provided by Dowell et al. (2004).

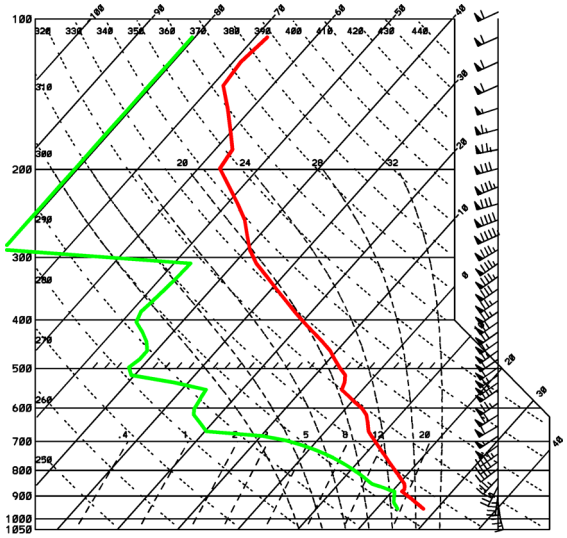

Figure 3. Sounding used in the data-assimilation and forecast experiments.

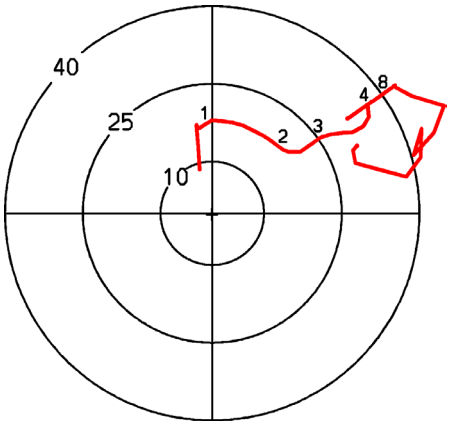

Figure 4. Hodograph corresponding to the sounding in Fig. 3. The rings indicate the wind speed in m s^{-1}. Heights (km AGL) are also plotted.

3. EnKF ANALYSES AND FORECASTS

Examples of the ensemble-mean analysis resulting from the assimilation of 6 observation volumes over a period of nearly 40 min are shown in Figs. 5 and 6. Three of several convective cells in central Oklahoma are highlighted in the figures. The cell in location "A" was the first significant cell in central Oklahoma during the afternoon of 8 May 2003. (This cell is 80 km southwest of the radar in the upper panel of Fig. 1). However, at 2124 UTC, the EnKF analysis indicates that the reflectivity echo in location "A" is not associated with any remaining updraft (Figs. 5 and 6).

Farther northwest, where the larger, higher-reflectivity core is located, the EnKF analysis indicates updrafts in locations "B" and "C" (Figs. 5 and 6). Of these, the updraft in location "B" is much stronger. At 2 km AGL, the "B" updraft is associated with strong cyclonic rotation, whereas the "C" updraft lies between regions of cyclonic and anticyclonic rotation. Hereafter, the updraft in location "B" and its reflectivity core will be referred to as the "main cell", and the updraft in location "C" and its reflectivity lobe will be referred to as the "left-flank cell".

We produced a forecast by initializing the model with the ensemble-mean analysis at 2126 UTC and then integrating the model 40 min, without assimilating additional observations. (We also integrated all ensemble members 40 min and will describe the mean and standard deviation of these forecasts in a later paper.) Examples of the forecast are shown in Figs. 7 and 8. Between 2126 and 2134 UTC, the model predicted some aspects of the observed storm evolution. First, the model correctly predicted the dissipation of cell "A" (the remnant low-reflectivity core of cell "A" is just southwest of the OUN radar in Fig. 7). Second, the model correctly indicates some separation of the left-flank cell [near (-30, 14) in Fig. 7] from the main cell, although both its maximum reflectivity and degree of separation from the main cell are underpredicted. Third, the model correctly predicted the formation of a hook echo at 2 km AGL on the southwest side of the maturing main cell. However, the model indicates a thin, low-reflectivity hook, whereas the observations indicate a wide, higher-reflectivity hook. In the actual storm, a series of small cells formed along the dryline to the southwest of the main cell and merged with the hook region of the main cell, increasing the reflectivity in the hook region. This storm evolution is not predicted in the model and highlights an important deficiency in our experiment.

The Oklahoma City storm produced an F0 tornado from 2204 to 2208 UTC, and an F0-F4 tornado from 2210 to 2238 UTC. We integrated the model 38 min, to the beginning time of the former tornado (Fig. 8). A mature supercell develops in the model, and at 2204 UTC, there is a hook echo associated with strong rotation at 2 km AGL. The hook echo in the model is located only 7 km from the observed hook echo. The model also predicts the formation of another left-flank cell (Fig. 8); this new left-flank cell is different from the one described previously in location "C" (Fig. 5), which has moved to the left and weakened.

Although some aspects of storm evolution are predicted well, there are some obvious deficiencies in the model forecast. First, the precipitation core in the modeled storm is too small (Fig. 8), indicating possible

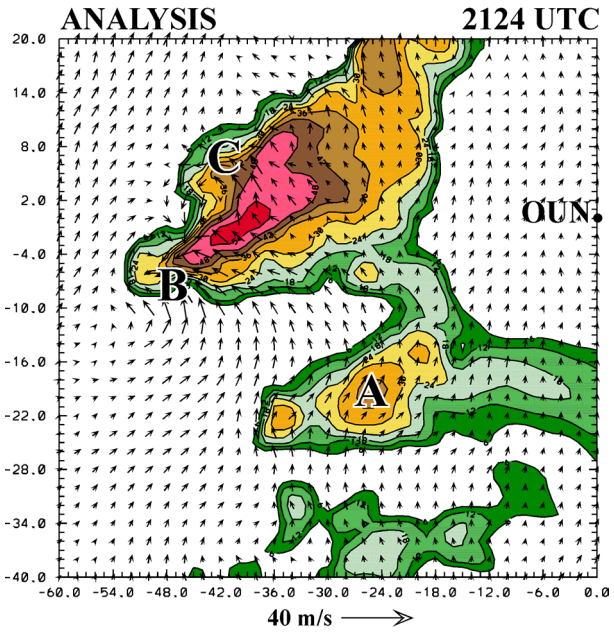

Figure 5. EnKF analysis of reflectivity (contours and shading at intervals of 6 dBZ$_e$) at 2124 UTC at 2.0 km AGL in a 60 km × 60 km portion of the 150 km × 150 km domain. Horizontal storm-relative winds are also shown. The letters "A", "B", and "C" refer to cell locations mentioned in the text.

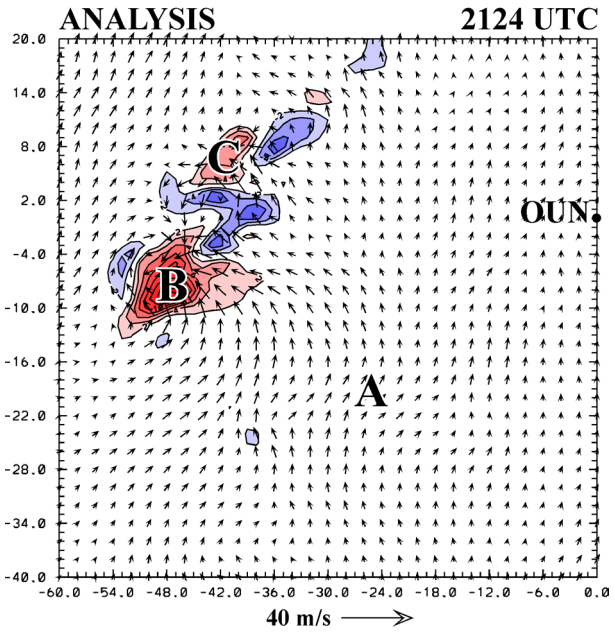

Figure 6. As in Fig. 5, except for vertical velocity (contours and shading at intervals of 2 m s^{-1}; updraft in red, downdraft in blue).

errors in the representation of precipitation microphysics in the model. Second, the peak low-level rotation in the model occurs at 2155 UTC (not shown), whereas the observed peak tornado intensity occurred after 2210 UTC.

4. DISCUSSION AND PLANS FOR FUTURE WORK

Storm-scale EnKF data assimilation provides the opportunity to extract additional information from observations; this additional information is valuable for storm research and will be valuable for operational nowcasting and warning when a real-time EnKF analysis system is available. The 3D wind analysis (Fig. 6) that was obtained by assimilating only single-Doppler observations provides an example of the value of a storm-scale EnKF analysis system. Specifically, there is an obvious signal for strong updraft in location "B" that in this case would have correctly drawn a forecaster's attention to an area of current concern and later concern downstream.

Storm-scale forecasting represents a greater challenge than storm-scale analysis. Given the limitations of the current experiment, the ability of the assimilation to identify the strong updraft of the developing supercell and the ability of the model to predict 40 min later the mature supercell's location within 7 km could be viewed with some encouragement. However, as discussed previously, there is room for improvement in the forecast for this case.

In future studies, we plan to investigate the sensitivity of the assimilation and forecast results to both the environmental sounding estimate and the precipitation microphysical scheme in the model. In addition, we plan to use a multi-scale approach to assimilate both radar data and environmental (e.g., Oklahoma Mesonet) data. By modeling the variability in the storm's environment associated with the dryline and other mesoscale features, we hope to improve the forecasts of the Oklahoma City storm.

ACKNOWLEDGMENTS

This study was supported by National Science Foundation grant ATM-0333872. We appreciate input by Chris Snyder. We thank Kevin Scharfenberg and Gordon Carrie for providing the KOUN radar data.

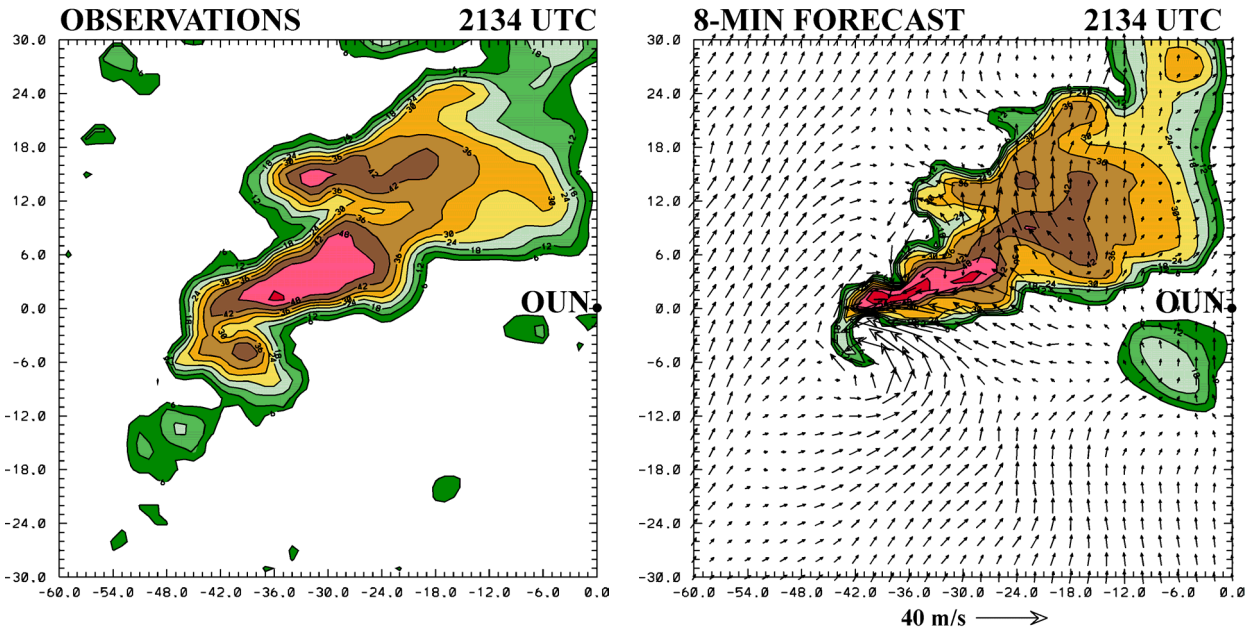

Figure 7. Observed (left) and model-forecast (right) reflectivity (contours and shading at intervals of 6 dBZ_e) at 2134 UTC at 2.0 km AGL in a 60 km × 60 km portion of the 150 km × 150 km domain. Horizontal storm-relative winds in the model are also shown.

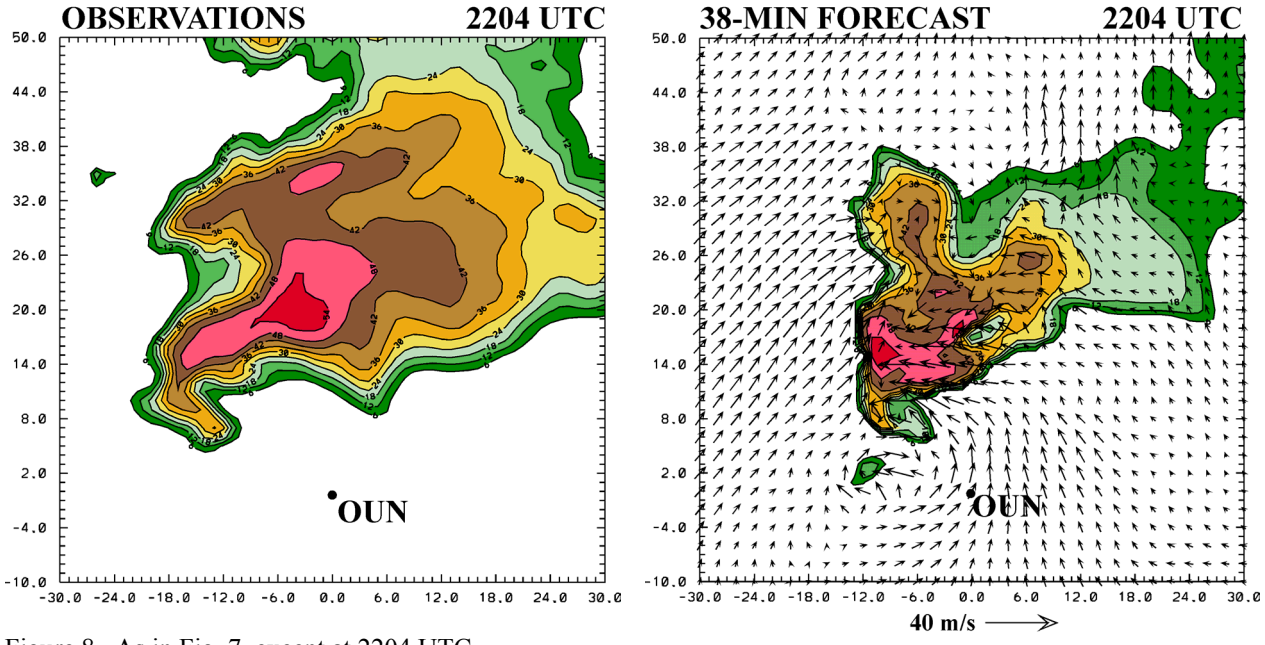

Figure 8. As in Fig. 7, except at 2204 UTC.

REFERENCES

Burgess, D. W., 2004: High resolution analyses of the 8 May 2003 Oklahoma City storm. Part I: Storm structure and evolution from radar data. Preprints, *22nd Conf. Severe Local Storms*, Hyannis, MA, Amer. Meteor. Soc., this volume.

Dowell, D. C., F. Zhang, L. J. Wicker, C. Snyder, and N. A. Crook, 2004: Wind and temperature retrievals in the 17 May 1981 Arcadia, Oklahoma, supercell: Ensemble Kalman filter experiments. *Mon. Wea. Rev*., **132**, 1982-2005.

Evensen, G., 1994: Sequential data assimilation with a nonlinear quasi-geostrophic model using Monte-Carlo methods to forecast error statistics. *J. Geophys. Res*., **99** (C5), 10143-10162.

Gilmore, M. S., J. M. Straka, and E. N. Rasmussen, 2004: Precipitation and evolution sensitivity in simulated deep convective storms: Comparisons between liquid-only and simple ice and liquid phase microphysics. *Mon. Wea. Rev*., **132**, 1897-1916.

Houtekamer, P. L., and H. L. Mitchell, 1998: Data assimilation using an ensemble Kalman filter technique. *Mon. Wea. Rev*., **126**, 796-811.

Lin, Y.-L., R. D. Farley, and H. D. Orville, 1983: Bulk parameterization of the snow field in a cloud model. *J. Appl. Meteor*., **22,** 1065-1092.

Snyder, C., and F. Zhang, 2003: Assimilation of simulated Doppler radar observations with an ensemble Kalman filter. *Mon. Wea. Rev*., **131**, 1663-1677.

Tong, M., and M. Xue, 2004: Ensemble Kalman filter assimilation of Doppler radar data with a compressible nonhydrostatic model: OSS Experiments. *Mon. Wea. Rev*., in review.

Wicker, L. J., and R. B. Wilhelmson, 1995: Simulation and analysis of tornado development and decay within a three-dimensional supercell thunderstorm. *J. Atmos. Sci*., 52, 2675-2703.

Zhang, F., C. Snyder, and J. Sun, 2004: Impacts of initial estimate and observation availability on convective-scale data assimilation with an ensemble Kalman filter. *Mon. Wea. Rev*., **132**, 1238-1253.